

# A Novel of PTA/ZIF-8@Cellulose Aerogel Composite Materials for Efficient Photocatalytic Degradation of Organic Dyes in Water

Jinguli Wen,<sup>[a]</sup> Huajian Liu,<sup>[a]</sup> Yili Zheng,<sup>[a]</sup> Yuhang Wu,<sup>[a]</sup> and Junkuo Gao\*<sup>[a]</sup>

**Abstract.** A novel PTA/ZIF-8@CA composite material (PTA = phosphotungstic acid; CA = cellulose aerogel) with multilayer three-dimensional network structure was synthesized with cellulose aerogel as the framework and MOFs as the filler. The results showed that the degradation rates of methylene blue at  $\delta = 10$  ppm reached 99.8% respectively in 30 min under the conditions of PTA/ZIF-8@CA input amount of  $0.6 \text{ g}\cdot\text{L}^{-1}$  and pH = 5. The degradation rate of rhodamine B at  $\delta =$

10 ppm reached 99.7% in 60 min. This shows that PTA/ZIF-8@CA has excellent degradation efficiency and short-term performance. In addition, after 5 photocatalytic cycles, the degradation rates of methylene blue and rhodamine B by PTA/ZIF-8@CA were still 83.0% and 82.5%, respectively, reflecting that PTA/ZIF-8@CA has terrific photocatalysis stability.

## 1 Introduction

Printing and dyeing wastewater is one of the culprits in polluting water resources in the natural environment. In the process of rapid economic development, reports on major pollution accidents caused by industrial discharge of printing and dyeing wastewater occur from time to time. Printing and dyeing wastewater contains a large amount of untreated organic dyes. Most of the organic dyes are chemically stable and not easily biodegradable in water, which has potential harm to the ecological environment.<sup>[1]</sup> Environmental pollution caused by organic dyes not only cannot be biodegraded, but also has carcinogenic, teratogenic and mutagenic hazards to organisms.<sup>[2]</sup> Currently, most of the wastewater treatment technologies widely used in industry are chlorination, but the by-products produced in them are mutagenic and carcinogenic to human health.<sup>[3]</sup> Other water treatment methods, such as chemical and membrane technologies, often involve high operating costs and sometimes generate other toxic secondary pollutants.<sup>[4]</sup> Therefore, the development of a green, efficient, and recyclable printing and dyeing wastewater purification treatment material is an urgent problem in the industry.

At present, the use of photocatalysts to degrade organic pollutants is considered as an effective way to treat printing and dyeing wastewater.<sup>[5]</sup> Photocatalysts can directly degrade organic pollutants into low-molecular or non-toxic small molecular substances under sunlight, or even completely decompose into carbon dioxide and water.<sup>[6]</sup> However, nano-semiconductor photocatalysts have the disadvantages of being easy to agglomerate and difficult to recycle, which will affect their photocatalytic performance in practical applications.<sup>[7]</sup> Phos-

photungstic acid is a new type of multifunctional catalyst with excellent photocatalytic activity and good stability.<sup>[8]</sup> However, phosphotungstic acid has a low surface area and is difficult to separate from the reaction impurity mixture, thus limiting the industrial application of phosphotungstic acid.<sup>[9]</sup> We think that it is possible to find a support for loading, which not only improves the disadvantage of not being able to be separated from impurities, but also further increases the catalytic active surface area. Cellulose aerogel has a high specific surface area and a wide pore size distribution, and is a good matrix carrier. However, most of the phosphotungstic acid contains oxygen-containing functional groups, which makes it difficult to graft onto cellulose aerogel.<sup>[10]</sup>

Metal-organic frameworks (MOFs) are a new type of inorganic-organic hybrid materials. Due to its high specific surface area and porosity, it has received widespread attention in recent years in the fields of catalysis, sensing, and gas adsorption.<sup>[11]</sup> Moreover, more and more researches have been conducted on the use of MOFs and their derivatives and the synthesis of related photocatalysts.<sup>[12]</sup> MOF-5,<sup>[13]</sup> MIL-101,<sup>[14]</sup> MIL-88,<sup>[15]</sup> NTU-9,<sup>[16]</sup> UIO-66,<sup>[17]</sup> etc. have all been explored for photocatalysis under certain conditions. *Jing* et al. proved that ZIF-8 can be used as an efficient photocatalyst for the decomposition of methylene blue.<sup>[18]</sup> *Ai* et al. found that MIL-53 series can decompose methylene blue and rhodamine under the action of visible light.<sup>[19]</sup> In order to further improve the photocatalytic performance of MOFs, semiconductor functional materials (TiO<sub>2</sub>, etc.) with photocatalytic activity are compounded with MOFs.<sup>[20]</sup> However, the particles of these materials are small and difficult to collect for secondary use, and are not suitable for practical water purification treatment applications.<sup>[21]</sup>

Therefore, in this paper, PTA/ZIF-8@CA composite materials with multilayer three-dimensional network structure were prepared by using cellulose aerogel as the framework and MOFs as the filler. Preparation process is shown in Figure 1. The degradation rates of methylene blue and rhodamine B by PTA/ZIF-8@CA under different conditions (pH value, initial concentration, and amount of photocatalyst added) was investi-

\* J. Gao

E-Mail: jkgao@zstu.edu.cn

[a] Institute of Functional Porous Materials  
School of Materials Science and Engineering  
Zhejiang Sci-Tech University  
Hangzhou 310018, P. R. China

Supporting information for this article is available on the WWW under <http://dx.doi.org/10.1002/zaac.202000096> or from the author.

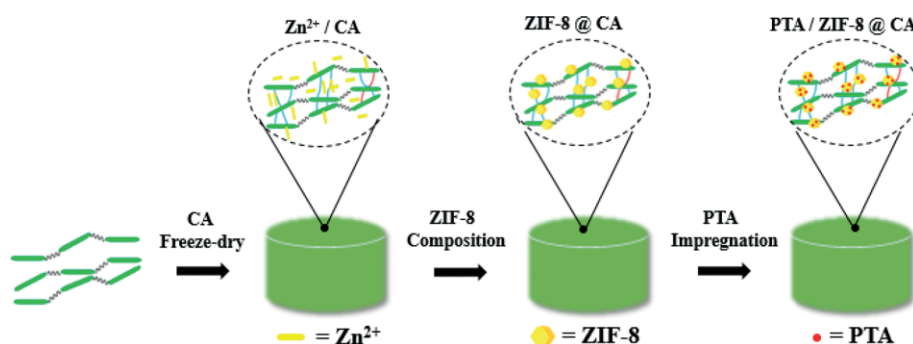


**Figure 1.** Schematic illustration of the synthetic process of PTA/ZIF-8@CA.

gated. The experimental results show that the degradation rates of methylene blue at  $\delta = 10$  ppm reached 99.8 % respectively in 30 min under the conditions of PTA/ZIF-8@CA input amount of  $0.6 \text{ g}\cdot\text{L}^{-1}$  and  $\text{pH} = 5$ . The degradation rate of rhodamine B at  $\delta = 10$  ppm reached 99.7 % in 60 min. In addition, after 5 photocatalytic cycles, the degradation rates of methylene blue and rhodamine B by PTA/ZIF-8@CA were still 83.0 % and 82.5 %. In terms of photocatalytic degradation of organic dyes, PTA/ZIF-8@CA shows excellent performance in high degradation efficiency and short time. This provides a new idea for the future synthesis of photocatalytic composites.

## 2 Results and Discussion

### 2.1 Characterization Analysis

The infrared spectrum analysis results of PTA/ZIF-8@CA are shown in Figure 2a and b. The stretching vibration peak of

C–H bond in the imidazole ring appeared at  $3198 \text{ cm}^{-1}$ .  $2888 \text{ cm}^{-1}$  is the characteristic absorption peak of cellulose molecules. The absorption peak at  $1645 \text{ cm}^{-1}$  is due to a small amount of water. The absorption peaks appearing near  $1545 \text{ cm}^{-1}$  are N–H bond bending vibrational absorption peaks. The absorption peak at  $1430 \text{ cm}^{-1}$  is the vibrational peak of the N–H bond in 2-methylimidazole. The absorption peak at  $1140 \text{ cm}^{-1}$  is the characteristic absorption peak of P–O. The absorption peak at  $990 \text{ cm}^{-1}$  is the characteristic absorption peak of W=O. The absorption peak at  $850 \text{ cm}^{-1}$  is the characteristic absorption peak of C–O–C. The absorption peak at  $755 \text{ cm}^{-1}$  is the characteristic absorption peak of W–O–W.

This shows that the process of preparing PTA/ZIF-8@CA did not destroy the cellulose skeleton and the crystal structure of ZIF-8, and introduced a large number of oxygen-containing functional groups, that is, PTA was successfully deposited on ZIF-8@CA. It can be seen from Figure 2c that the PTA/ZIF-8 and PTA/ZIF-8@CA diffraction peaks at (011), (002), (112),

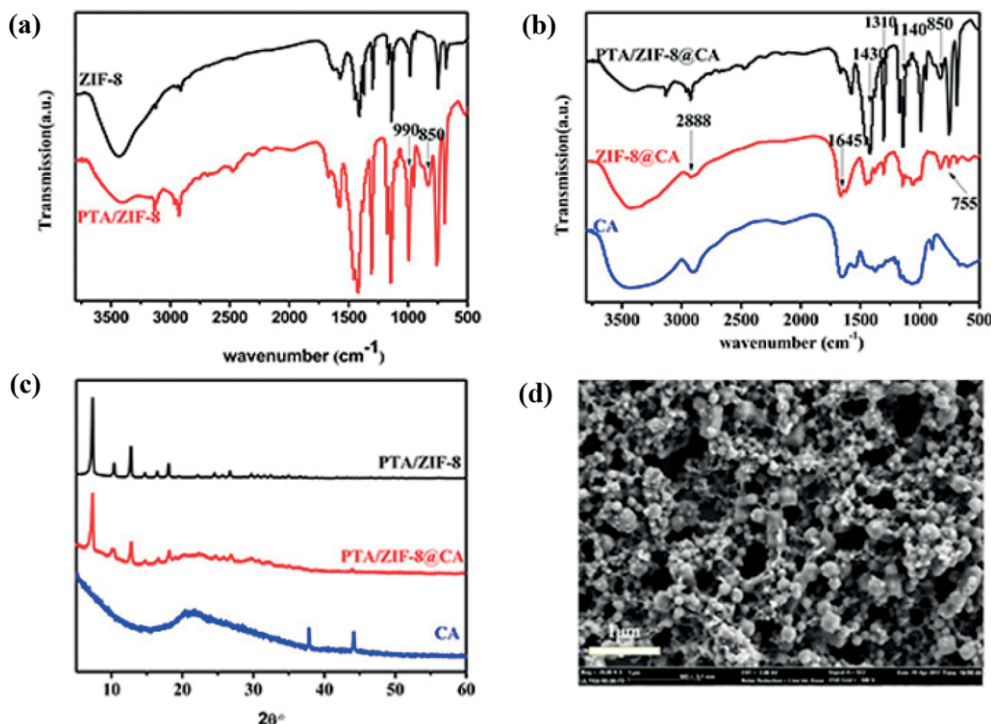


**Figure 2.** (a and b) FT-IR chart of PTA/ZIF-8@CA; (c) XRD pattern of PTA/ZIF-8@CA; (d) SEM image of PTA/ZIF-8@CA.

(222) are basically unchanged. (020) is a typical cellulose diffraction peak, which indicates that the crystal strength of PTA and ZIF-8 in PTA/ZIF-8@CA has not been destroyed. This further proves that PTA and ZIF-8 are successfully compounded with cellulose aerogels. The morphological structure of PTA/ZIF-8@CA is shown in Figure 2d. After the cellulose molecular chains are crosslinked by the MBA, a three-dimensional porous structure is formed that is significantly interconnected. ZIF-8 attached to the cellulose pores in the composite showed different hierarchical porous structures, while PTA was supported on the surface of ZIF-8. This indicates that the prepared PTA/ZIF-8@CA has a multilayer three-dimensional network structure.

## 2.2 Photocatalytic Degradation Performance Analysis

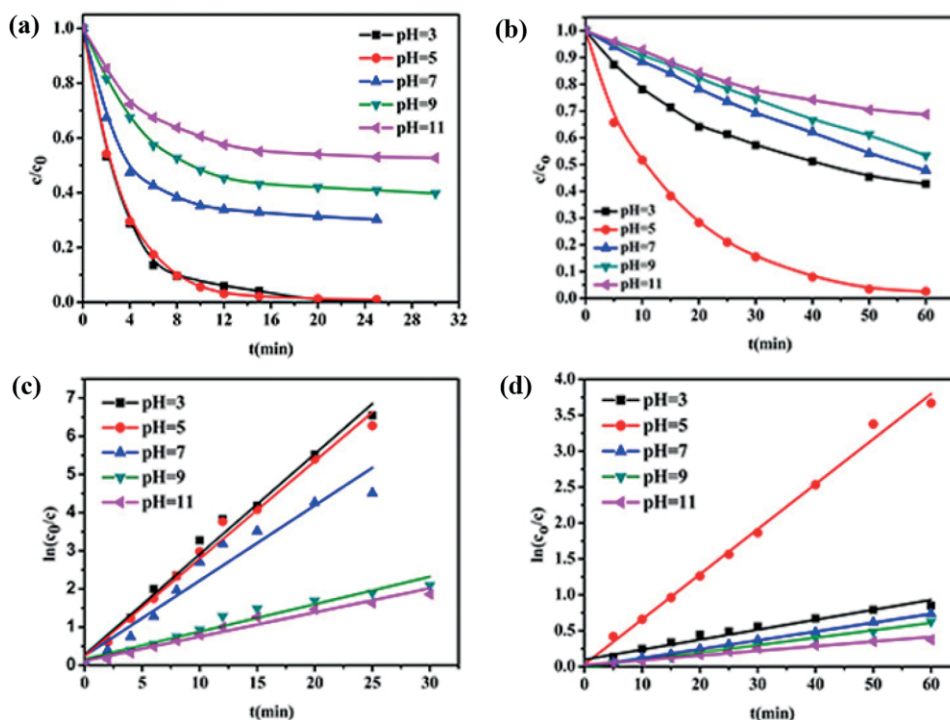
### 2.2.1 Effect of pH

Figure 3 shows the photocatalytic degradation curves and kinetic equations of 120 mg PTA/ZIF-8@CA samples in 25 mL, 10 ppm methylene blue and rhodamine B solutions at different pH conditions. It can be seen from Figure 3a and b that the degradation rates of methylene blue and rhodamine B by PTA/ZIF-8@CA under different pH conditions changes with the change of the system pH value, and with acidic conditions the photocatalytic degradation efficiency is better. This is because acidity promotes photocatalysis, but strong acids can cause ZIF-8 to collapse. Therefore, the photodegradation rate of methylene blue and rhodamine B reached the best at pH = 5. After 30 minutes of photocatalysis, the degradation rate of methylene blue by PTA/ZIF-8@CA reached 99.8% at pH =

5. After 60 minutes of photocatalysis, the degradation rate of rhodamine B by PTA/ZIF-8@CA reached 99.7%. At the same time, Figure 3c and d show the Langmuir-Hinshelwood relationship curves of the two dyes, and the linear fitting correlation coefficients  $R^2$  are greater than 0.9. This shows that the degradation of methylene blue and rhodamine B by PTA/ZIF-8@CA accords with pseudo-first-order kinetics. After 30 minutes of photocatalysis, the degradation rate of methylene blue by PTA/ZIF-8@CA reached 99.8% at pH = 5, and the reaction rate constant ( $k = 0.338$ ) was the largest. After 60 minutes of photocatalysis, the degradation rate of rhodamine B by PTA/ZIF-8@CA reached 99.7%, and the reaction rate constant ( $k = 0.068$ ) was the largest. But PTA/ZIF-8@CA had the lowest degradation rate of the two organic dyes at pH = 11, and the rate constant ( $k = 0.052, 0.0012$ ) was the smallest. This is because acidity promotes photocatalysis, and  $H^+$  can effectively capture photogenerated electrons during photocatalysis. However, strong acids can also cause ZIF-8 to collapse, leading to unstable catalytic systems. Therefore, the pH of the methylene blue and rhodamine B prepared by the photocatalytic degradation reaction is generally about 5 to be the best. Under these conditions, PTA/ZIF-8@CA has higher photodegradation rate and better stability.

### 2.2.2 Effect of Initial Concentration

The effect of the initial concentration of methylene blue and rhodamine B on the photocatalytic degradation rate is shown in Figure 4 below. It can be seen from Figure 4a and b that after 20 minutes of photocatalytic degradation, the degradation



**Figure 3.** Effect of pH on degradation rate (a) degradation curve of methylene blue; (b) degradation curve of rhodamine B; (c) degradation kinetics curve of methylene blue; (d) degradation kinetics curve of rhodamine B.

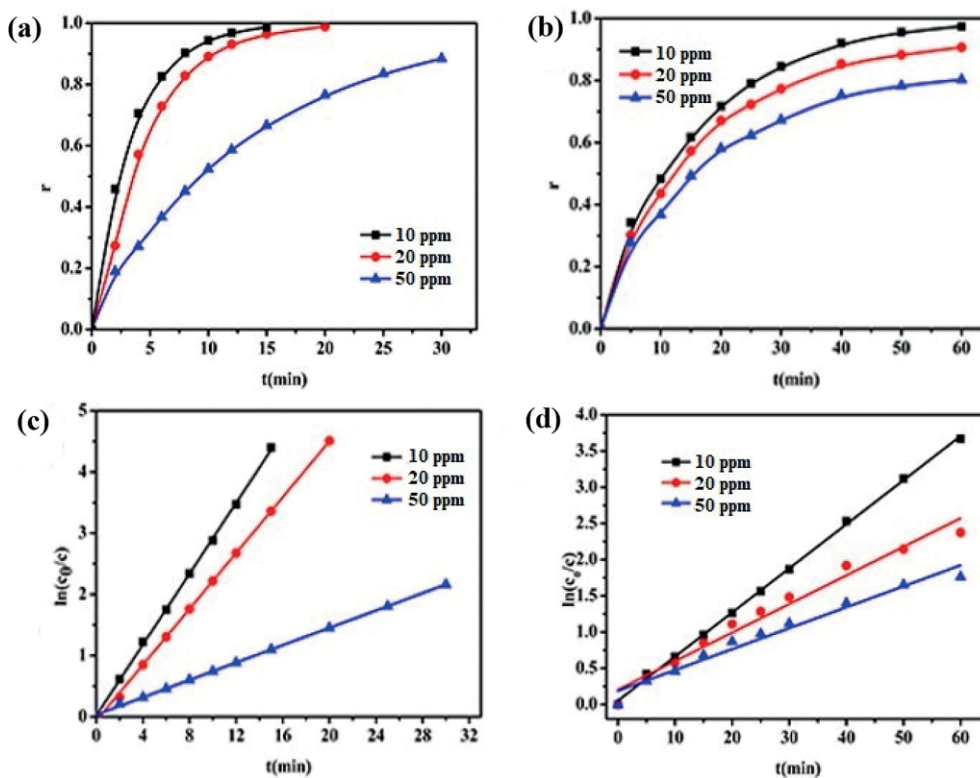


**Figure 4.** Effect of initial concentration on degradation rate (a) degradation curve of methylene blue; (b) degradation curve of rhodamine B; (c) degradation curve of methylene blue; (d) degradation kinetics of rhodamine B.

rates of 10 ppm methylene blue and rhodamine B by PTA/ZIF-8@CA were 99.8% and 99.7%, respectively. The degradation rates of PTA/ZIF-8@CA to 50 mg·L<sup>-1</sup> of methylene blue and rhodamine B were reduced to 87.3% and 73.2%. This shows that the initial concentration of methylene blue and rhodamine B has a certain effect on the degradation rate. From the kinetic curves of Figure 4c and d, it can be seen that the reaction rate constant ( $k_1 = 0.353$ ,  $k_2 = 0.061$ ) of PTA/ZIF-8@CA for the degradation of 10 ppm methylene blue and rhodamine B is the largest. The linear fitting correlation coefficients  $R^2$  are all greater than 0.9, and it can be considered that the degradation process conforms to pseudo-first-order kinetics. When the concentration of methylene blue and rhodamine B increased, the reaction rate gradually decreased. When the concentration of methylene blue and rhodamine B was 50 ppm, the reaction rate constants ( $k_1 = 0.073$ ,  $k_2 = 0.033$ ) were reduced to a minimum. There are several reasons for this: (1) The higher the concentration of pollutants, the weaker the ability of light to penetrate the solution, resulting in fewer photons participating in the catalytic oxidation reaction; (2) The higher the concentration of the pollutants, the more the methylene blue and rhodamine B particles adsorbed on the surface of PTA/ZIF-8@CA, resulting in a decrease in available photocatalytic active sites. Therefore, the number of photo-generated electrons and hole pairs generated in per unit time also decreases; (3) The higher the concentration of the pollutants, the intermediate products generated by the reaction may be re-adsorbed on the catalyst surface before they can be completely decomposed. It is easy to react in reverse to form the initial structural forms of meth-

ylene blue and rhodamine B. Therefore, when the initial concentrations of the methylene blue and rhodamine B are increased, the reaction time is prolonged and the degradation rate is slowed.

### 2.2.3 Effect of Dosage

Figure 5 shows the photocatalytic degradation curves and kinetic curves of different amounts of PTA/ZIF-8@CA in 10 ppm methylene blue and rhodamine B. It can be seen from Figure 5 that the input amount of PTA/ZIF-8@CA has an important influence on the photocatalytic reaction of methylene blue and rhodamine B. When the input amount of PTA/ZIF-8@CA is 0.2 g·L<sup>-1</sup>, the photocatalytic degradation rates of 10 ppm methylene blue and rhodamine B are 91.1% and 92.4%, respectively. When the input amount was increased to 0.4 g·L<sup>-1</sup>, the photocatalytic degradation rates of methylene blue and rhodamine B reached 98.7% and 97.4%. After further increasing to 0.6 g·L<sup>-1</sup>, the photocatalytic degradation rates of methylene blue and rhodamine B reached 99.98% and 98.7%. It can be seen from Figure 5b that the linear fitting correlation coefficients  $R^2$  are also greater than 0.9, and it can be considered that the degradation process conforms to pseudo-first-order kinetics. With the increase in the amount of PTA/ZIF-8@CA, the reaction rate gradually increased. This may be related to the absorption of light. Because as the amount of catalyst increases, the absorption and utilization of light also increases, so the reaction rate also increases. However, as the amount of catalyst further increases to a certain

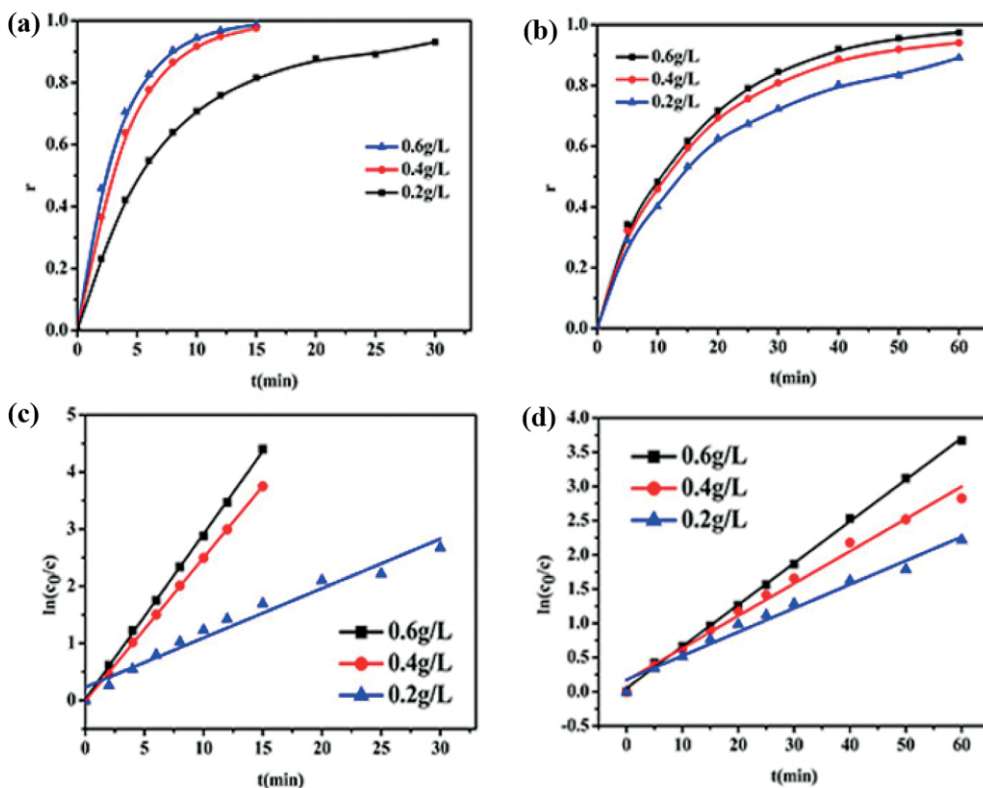


**Figure 5.** Effect of photocatalyst input on degradation rate (a) degradation curve of methylene blue; (b) degradation curve of rhodamine B; (c) degradation curve of methylene blue; (d) degradation kinetics curve of rhodamine B.

level, the available light energy will be less and less. In addition, the loss of light energy caused by the catalyst's reflection, shielding, and scattering of light will increase, resulting in longer reaction time and slower degradation rate.

### 2.3 Photocatalytic Cyclability and Catalytic Mechanism Analysis

For practical applications, the photocatalytic stability of photocatalytic materials is a very important factor. Figure 6 is the curve of 5 cycles of catalyzing 25 mL of  $10 \text{ mg}\cdot\text{L}^{-1}$  methylene blue and rhodamine B solution at  $120 \text{ mg}$  PTA/ZIF-8@CA. The degradation rates of methylene blue solution by PTA/ZIF-8@CA were 99.8%, 96.6%, 94.5%, 92.5%, and 83.0%. The degradation rates of rhodamine B solution by PTA/ZIF-8@CA were 99.7%, 95.4%, 92.5%, 90.3%, and 82.5%. The experimental results show that with the increase in the number of times PTA/ZIF-8@CA is used, the degradation efficiency shows a gradual decline, but the decline is not very obvious. This shows that the photocatalytic performance of the prepared PTA/ZIF-8@CA is relatively stable, and has certain potential application value in practical applications.

When phosphotungstic acid absorbs photons, the energy of the valence band electrons rises to the conduction band, thereby forming photogenerated electron-hole pairs.  $\text{P}_2\text{W}_{18}$  can efficiently receive and transfer electrons, which are beneficial to improve the separation efficiency of photogenerated electron-hole pairs, thereby improving the photocatalytic effi-

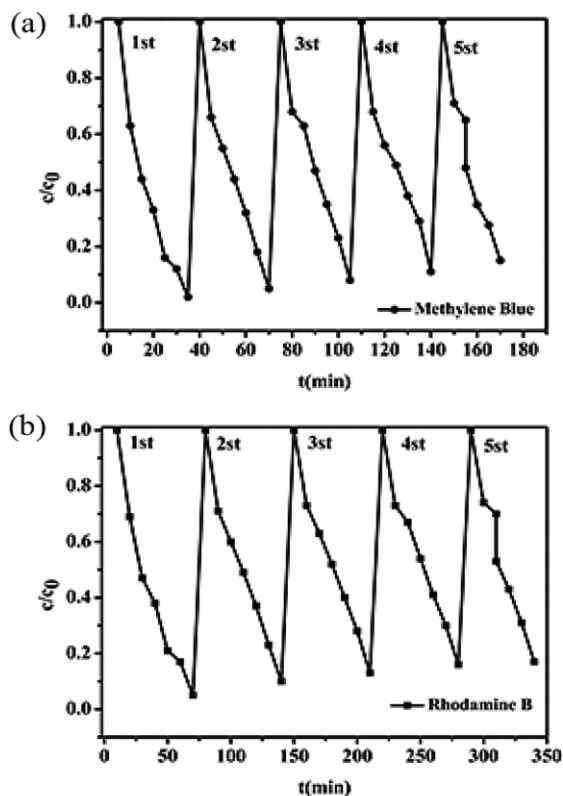


**Figure 6.** PTA/ZIF-8@CA photocatalytic degradation cycle curve (a) methylene blue; (b) rhodamine B.

ciency. Photogenerated electron–hole pairs are separated by the electric field or diffusion and migrate to the surface of PTA/ZIF-8@CA. The electrons migrated to the surface undergo oxidation-reduction reaction with the organic dye pollutants adsorbed by PTA/ZIF-8@CA, thereby achieving efficient photocatalytic degradation of the organic dye pollutants.

### 3 Conclusions

In summary, a new multilayer PTA/ZIF-8@CA composite material with cellulose aerogel as the framework and MOFs materials as the filler was successfully synthesized. Characterization showed that not only did not destroy the cellulose skeleton and the crystal structure of ZIF-8, but also introduced a large amount of phosphotungstic acid during the preparation of PTA/ZIF-8@CA. The results of photocatalytic degradation experiments proved that pH, the initial concentration of methylene blue and rhodamine B, and the input amount of PTA/ZIF-8@CA all had certain effects on the photocatalytic degradation of methylene blue and rhodamine B. The degradation rates of methylene blue at  $\delta = 10$  ppm reached 99.8% in 30 minutes under the conditions of PTA/ZIF-8@CA input amount of  $0.6 \text{ g}\cdot\text{L}^{-1}$  and  $\text{pH} = 5$ . The degradation rate of rhodamine B at  $\delta = 10$  ppm reached 99.7% in 60 minutes. This shows that PTA/ZIF-8@CA has excellent performance of high degradation efficiency and short time. In addition, after 5 photocatalytic cycles, the degradation rates of methylene blue and rhodamine B by PTA/ZIF-8@CA were still 83.0% and 82.5%, reflecting that PTA/ZIF-8@CA has terrific photocatalysis stability.

**Supporting Information** (see footnote on the first page of this article): The Experimental Section.

### Acknowledgements

This work was supported by the Zhejiang Provincial Natural Science Foundation of China (LY20E020001) and the National Natural Science Foundation of China (51602301 and 51672251). J.G. acknowledges the Fundamental Research Funds of Zhejiang Sci-Tech University (2019Q007).

**Keywords:** Metal-organic frameworks; Cellulose; Aerogel; Phosphotungstic acid; Photocatalysis

### References

- [1] a) L. X. G Liu, J. Zhao, et al., *Environ. Sci. Technol.* **2000**, *34*, 3982–3990; b) W. E. J. Baughman, *Environ. Sci. Technol.* **1994**, *28*, 267–276; c) A. A. Adeyemo, I. O. Adeoye, O. S. Bello, *Toxicol. Environ. Chem.* **2012**, *94*, 1846–1863; d) J. Levec, A. Pintar, *Catal. Today* **2007**, *124*, 172–184.
- [2] a) U. I. Gaya, A. H. Abdullah, *J. Photochem Photobiol. C* **2008**, *9*, 1–12; b) W. T. Tsai, H. C. Hsu, T. Y. Su, K. Y. Lin, C. M. Lin, T. H. Dai, *J. Hazard. Mater.* **2007**, *147*, 1056–1062; c) J. Zhao, J. Wong, C. Wang, J. Gao, V. Ng, H. Y. Yang, S. C. J. Ioo, Q. Zhang, *Chem. Asian J.* **2013**, *8*, 665–669; d) J. Gao, Y. Cui, J. Yu, W. Lin, Z. Wang, G. Qian, *J. Mater. Chem.* **2011**, *21*, 3197–3203.
- [3] a) M. N. Chong, B. Jin, C. W. Chow, C. Saint, *Water Res.* **2010**, *44*, 2997–3027; b) H. Yang, H. Cheng, *Sep. Purif. Technol.* **2007**, *56*, 392–396.
- [4] J. Lu, T. Zhang, J. Ma, Z. Chen, *J. Hazard. Mater.* **2009**, *162*, 140–145.
- [5] a) K. Inumaru, T. Ishihara, Y. Kamiya, T. Okuhara, S. Yamanaka, *Angew. Chem. Int. Ed.* **2007**, *46*, 7625–7628; b) M. S. Sampurnam S, Dhanasekaran T, et al., *J. Photochem Photobiol. A* **2019**, *370*, 26–40; c) H. J. Zhu, K. She, et al., *J. Am. Chem. Soc.* **2009**, *131*, 9715–9721.
- [6] a) G. R. Bertolini, L. R. Pizzio, A. Kubacka, M. J. Muñoz-Batista, M. Fernández-García, *Appl. Catal. B, Environ.* **2018**, *225*, 100–109; b) S. X. Guo, F. Li, L. Chen, D. R. MacFarlane, J. Zhang, *ACS Appl. Mater. Interfaces* **2018**, *10*, 12690–12697; c) C. Kato, K. Y. Maryunina, K. Inoue, S. Yamaguchi, H. Miyaoka, A. Hayaishi, M. Sadakane, R. Tsunashima, S. Nishihara, *Chem. Lett.* **2017**, *46*, 602–604.
- [7] a) A. Rey, E. Mena, A. M. Chávez, F. J. Beltrán, F. Medina, *Chem. Eng. Sci.* **2015**, *126*, 80–90; b) J. Romão, G. Mul, *ACS Catal.* **2016**, *6*, 1254–1262; c) H. F. Shi, G. Yan, Y. Zhang, H. Q. Tan, W. Z. Zhou, Y. Y. Ma, Y. G. Li, W. Chen, E. B. Wang, *ACS Appl. Mater. Interfaces* **2017**, *9*, 422–430.
- [8] a) L. Osiglio, G. Sathicq, L. Pizzio, G. Romanelli, M. Blanco, *J. Mol. Catal. A* **2017**, *426*, 88–96; b) J. Yang, N. Zhang, H. Li, B. Xu, W. Tian, D. Dong, *Polym. Int.* **2015**, *64*, 804–810; c) X.-Y. Yang, M.-T. Li, N. Sheng, J.-S. Li, G.-D. Liu, J.-Q. Sha, J. Jiang, *Cryst. Growth Des.* **2018**, *18*, 5564–5572.
- [9] a) U. Jameel, M. Zhu, X. Chen, Z. Tong, *J. Mater. Sci.* **2015**, *50*, 2181–2198; b) J.-Q. Sha, X. Li, J.-S. Li, X.-Y. Yang, H.-F. Zhang, M.-B. Yue, K. Zhou, *Cryst. Growth Des.* **2018**, *18*, 2289–2296; c) S. S. Wang, G. Y. Yang, *Chem. Rev.* **2015**, *115*, 4893–4962.
- [10] J. Yu, T. Wang, S. Rtimi, *Appl. Catal. B, Environ.* **2019**, *254*, 66–75.
- [11] a) H. Furukawa, K. E. Cordova, M. O’Keeffe, O. M. Yaghi, *Science* **2013**, *341*, 1230444; b) C. Li, H. Xu, J. Gao, W. Du, L. Shangguan, X. Zhang, R.-B. Lin, H. Wu, W. Zhou, X. Liu, J. Yao, B. Chen, *J. Mater. Chem. A* **2019**, *7*, 11928–11933; c) Y. Li, T. Zhao, M. Lu, Y. Wu, Y. Xie, H. Xu, J. Gao, J. Yao, G. Qian, Q. Zhang, *Small* **2019**, *15*, 1901940; d) L. Wang, H. Xu, J. Gao, J. Yao, Q. Zhang, *Coord. Chem. Rev.* **2019**, *398*, 213016; e) Y. Li, M. Lu, Y. Wu, H. Xu, J. Gao, J. Yao, *Adv. Mater. Interfaces* **2019**, *6*, 1900290.
- [12] a) S.-L. Li, Q. Xu, *Energy Environ. Sci.* **2013**, *6*, 1656–1683; b) C.-C. Wang, J.-R. Li, X.-L. Lv, Y.-Q. Zhang, G. Guo, *Energy Environ. Sci.* **2014**, *7*, 2831–2867; c) J. Zhao, X. Liu, Y. Wu, D.-S. Li, Q. Zhang, *Coord. Chem. Rev.* **2019**, *391*, 30–43; d) J. Zhao, W.-W. Dong, Y. Wu, C. Wang, D.-S. Li, Q. Zhang, *J. Mater. Chem. A* **2015**, *3*, 6962–6969; e) J. Gao, X. Qian, R. Lin, R. Krishna, H. Wu, W. Zhou, B. Chen, *Angew. Chem. Int. Ed.* **2020**, *59*, 4396–4400; f) J. Gao, J. Cong, Y. Wu, L. Sun, J. Yao, B. Chen, *ACS Appl. Energy Mater.* **2018**, *1*, 5140–5144; g) Q. Huang, J. Yu, J. Gao, X. Rao, X. Yang, Y. Cui, C. Wu, Z. Zhang, S. Xiang, B. Chen, *Cryst. Growth Des.* **2010**, *10*, 5291–5296; h) X. Qian, P. He, J. Chen, B. Wang, E. Lv, J. Gao, J. Yao, *Z. Anorg. Allg. Chem.* **2019**, *645*, 906–909.
- [13] M. Alvaro, E. Carbonell, B. Ferrer, F. X. Llabres i Xamena, H. Garcia, *Chem. Eur. J.* **2007**, *13*, 5106–5112.
- [14] J. He, Z. Yan, J. Wang, J. Xie, L. Jiang, Y. Shi, F. Yuan, F. Yu, Y. Sun, *Chem. Commun.* **2013**, *49*, 6761–6763.
- [15] W. T. Xu, L. Ma, F. Ke, F. M. Peng, G. S. Xu, Y. H. Shen, J. F. Zhu, L. G. Qiu, Y. P. Yuan, *Dalton Trans.* **2014**, *43*, 3792–3798.
- [16] J. Gao, J. Miao, P. Z. Li, W. Y. Teng, L. Wang, Y. Zhao, B. Liu, Q. Zhang, *Chem. Commun.* **2014**, *50*, 3786–3788.
- [17] Z. Yang, X. Tong, J. Feng, S. He, M. Fu, X. Niu, T. Zhang, H. Liang, A. Ding, X. Feng, *Chemosphere* **2019**, *220*, 98–106.
- [18] H.-P. Jing, C.-C. Wang, Y.-W. Zhang, P. Wang, R. Li, *RSC Adv.* **2014**, *4*, 54454–54462.
- [19] L. Ai, C. Zhang, L. Li, J. Jiang, *Appl. Catal. B Environ.* **2014**, *148–149*, 191–200.

[20] a) X. Li, Y. Pi, Q. Hou, H. Yu, Z. Li, Y. Li, J. Xiao, *Chem. Commun.* **2018**, 54, 1917–1920; b) Q. Liu, B. Zhou, M. Xu, G. Mao, *RSC Adv.* **2017**, 7, 8004–8010.

[21] a) J. Wen, P. He, C. Lei, E. Lv, Y. Wu, J. Gao, J. Yao, *J. Solid State Chem.* **2019**, 274, 26–31; b) C. Lei, J. Gao, W. Ren, Y. Xie, S. Y. H. Abdalkarim, S. Wang, Q. Ni, J. Yao, *Carbohydr. Polym.* **2019**, 205, 35–41; c) W. Ren, J. Gao, C. Lei, Y. Xie, Y. Cai, Q.

Ni, J. Yao, *Chem. Eng. J.* **2018**, 349, 766–774; d) S. Bo, W. Ren, C. Lei, Y. Xie, Y. Cai, S. Wang, J. Gao, Q. Ni, J. Yao, *J. Solid State Chem.* **2018**, 262, 135–141.

---

Received: February 25, 2020

Published Online: April 29, 2020